



**Calhoun: The NPS Institutional Archive**  
**DSpace Repository**

---

Faculty and Researchers

Faculty and Researchers' Publications

---

2018-06-22

Single-ended mid-infrared laser-absorption sensor for time-resolved measurements of water concentration and temperature within the annulus of a rotating detonation engine

Peng, Wen Yu; Cassady, Séan J.; Strand, Christopher L.; Goldenstein, Christopher S.; Spearrin, R. Mitchell; Brophy, Christopher M.; Jeffries, Jay B.; Hanson, Ronald K.

Elsevier

---

Peng, Wen Yu, et al. "Single-ended mid-infrared laser-absorption sensor for time-resolved measurements of water concentration and temperature within the annulus of a rotating detonation engine." *Proceedings of the Combustion Institute* 37.2 (2019): 1435-1443.



Downloaded from NPS Archive: Calhoun

<http://www.nps.edu/library>

Calhoun is the Naval Postgraduate School's public access digital repository for research materials and institutional publications created by the NPS community. Calhoun is named for Professor of Mathematics Guy K. Calhoun, NPS's first appointed -- and published -- scholarly author.

**Dudley Knox Library / Naval Postgraduate School**  
**411 Dyer Road / 1 University Circle**  
**Monterey, California USA 93943**

# Single-ended mid-infrared laser-absorption sensor for time-resolved measurements of water concentration and temperature within the annulus of a rotating detonation engine

Wen Yu Peng<sup>a,\*</sup>, Séan J. Cassady<sup>a</sup>, Christopher L. Strand<sup>a</sup>,  
Christopher S. Goldenstein<sup>b</sup>, R. Mitchell Spearrin<sup>c</sup>,  
Christopher M. Brophy<sup>d</sup>, Jay B. Jeffries<sup>a</sup>, Ronald K. Hanson<sup>a</sup>

<sup>a</sup> Department of Mechanical Engineering, Thermosciences Division, 452 Escondido Mall, Stanford University, California 94305, USA

<sup>b</sup> School of Mechanical Engineering, Purdue University, West Lafayette, Indiana 47907, USA

<sup>c</sup> Department of Mechanical and Aerospace Engineering, University of California, Los Angeles, California 90095, USA

<sup>d</sup> Department of Mechanical and Aerospace Engineering, Naval Postgraduate School, Monterey, California 93943, USA

Received 29 November 2017; accepted 1 May 2018

Available online 22 June 2018

## Abstract

A novel single-ended mid-infrared laser-absorption sensor for time-resolved measurements of water mole fraction and temperature was developed and deployed within the annulus of a hydrogen/air-fed rotating detonation engine (RDE). The sensor transmitted two laser beams targeting mid-infrared water transitions through a single optical port on the outer wall of the cylindrical RDE annulus and measured the backscattered radiation from the RDE inner surface using a photodetector for a round-trip path of 1.52 cm. Optimizing the sensor's optical arrangement using numerical ray tracing to minimize interference from optical emission, beam steering, and scattered laser light from window surfaces was essential to sensor performance. Scanned-wavelength-modulation spectroscopy with second-harmonic detection and first-harmonic normalization was implemented to allow for frequency-domain multiplexing of the two lasers and to suppress non-absorbing interference sources such as beam-steering and emission. Tunable diode lasers near 2551 and 2482 nm were modulated at 100 and 122 kHz, respectively, and sinusoidally scanned across the peaks of their respective water transitions at 10 kHz to provide a measurement rate of 20 kHz and detection limit of 0.5% water by mole. Experimentally derived spectroscopic parameters enabled water and temperature sensing with respective uncertainties of 7.3% and 5.3% relative to the measured values. Time-resolved and time-averaged sensor measurements of gas temperature and water vapor mole fraction allow quantitative evaluation of the combustion progress at the measurement location and thus provide a design tool for RDE

\* Corresponding author.

E-mail address: [wypeng@stanford.edu](mailto:wypeng@stanford.edu) (W.Y. Peng).

optimization. Broadly, this single-ended laser sensor should find applications in other combustion systems where optical access is limited.

© 2018 The Combustion Institute. Published by Elsevier Inc. All rights reserved.

**Keywords:** Single-ended; Combustion diagnostics; Mid-infrared; Wavelength-modulation spectroscopy; Detonations

## 1. Introduction

Rotating detonation engines (RDEs) have received considerable interest due to the thermodynamic advantages of detonative combustion, their ability to be continuously fed with reactants, and their high operating frequencies. A significant body of research has been published detailing numerical and experimental investigations into the RDE, many of which are summarized in [1,2]. Central to increasing the technological readiness of RDEs is the development of robust, time-resolved experimental diagnostics to bridge the gap between computational and practical design efforts.

Laser-absorption spectroscopy (LAS) in particular is a proven technology for non-intrusive, time-resolved, and species-specific sensing in harsh environments [3] such as pulsed-detonation engines [4], scramjets [5], and at the exit plane of an RDE [6]. These LAS applications involve transmitting monochromatic laser light through an absorbing medium and correlating the fractional transmission to desired gas properties. However, installing a direct optical path through an RDE combustion annulus is impractical and therefore single-ended LAS approaches relying on detection of back-reflected light from an inner RDE surface are preferred. Rein et al. used this approach in recent work [7,8] to perform single-ended 100 kHz measurements of water ( $\text{H}_2\text{O}$ ) vapor and temperature within a hydrogen ( $\text{H}_2$ )/air-fed RDE at multiple planes along the combustor. This sensor relied on detecting the back-reflection of a tunable laser source, targeting near-infrared (NIR,  $\lambda \sim 1.35 \mu\text{m}$ ) absorption transitions, from the inner annular surface of the RDE. Although these researchers did not quantify detection limits, previous comparisons between NIR and mid-infrared (MIR) sensors in an RDE [6] suggest that the use of stronger MIR transitions allows for a greater than 10-fold improvement in  $\text{H}_2\text{O}$  detection limits.

In this work, the development and deployment of a 20 kHz measurement rate single-ended two-color MIR sensor for monitoring temperature and  $\text{H}_2\text{O}$  mole fraction within the annulus of an early generation  $\text{H}_2$ /air-fed RDE combustor at the Naval Postgraduate School (NPS) is presented. The use of strong absorption transitions near  $2.5 \mu\text{m}$  in conjunction with the interference-tolerant wavelength-modulation spectroscopy (WMS) technique provided high signal-to-noise ratio (SNR) mea-

surements despite the short optical path of 1.52 cm within the combustor. The optical design is built on the fiber-based architecture in [9] and several additional difficulties unique to the single-ended strategy were addressed by using a ray-tracing optimization scheme.

Measurements were performed at various global equivalence ratios ( $\Phi_{\text{global}}$ ). The sensor identified transient operating dynamics including the primary detonation mode near 3 kHz competing against a natural acoustic mode near 2.3 kHz. Detonation velocities were found to accelerate with time at an average rate of  $54 \text{ m/s}^2$ . Time-averaged mole fractions and temperatures were weak functions of  $\Phi_{\text{global}}$ , indicating mixing-limited combustion near the injector with combustion progress at the measurement location averaging 35%. The detection limit at the mean RDE operating environment was 0.5%  $\text{H}_2\text{O}$  by mole while uncertainties were estimated to be 7.3% and 5.3% relative to the measured values for  $\text{H}_2\text{O}$  and temperature, respectively. To the authors' knowledge, this work represents the first time-resolved, single-ended MIR sensor for practical combustor environments. Additionally, the sensor design lays the foundation for additional short-path single-ended diagnostics probing the fundamental bands of common combustion species such as  $\text{CO}$ ,  $\text{CO}_2$ , and  $\text{NO}$  which can be difficult to detect using NIR transitions.

## 2. Theory

### 2.1. Laser-absorption

The fractional transmittance, defined as the ratio between the transmitted ( $I_t$ ) and incident ( $I_0$ ) intensities, of monochromatic radiation with frequency  $\nu$  ( $\text{cm}^{-1}$ ) through a uniform ideal gas is described by the Beer-Lambert relation:

$$\left(\frac{I_t}{I_0}\right)_\nu = \exp(-\alpha_\nu) = \exp\left\{-\sum_j S_j P \chi L \phi_{\nu,j}\right\} \quad (1)$$

Here,  $S_j$  ( $\text{cm}^2/\text{atm}$ ) is the line-strength of the  $j^{\text{th}}$  absorbing transition,  $P$  (atm) is the total gas pressure,  $\chi$  is the mole fraction of the absorbing species,  $L$  (cm) is the optical path length, and  $\phi_{\nu,j}$  (cm) is the lineshape of the  $j^{\text{th}}$  absorbing transition.

The Voigt lineshape function, which accounts for Doppler and collisional broadening effects, was used to model  $\phi_{v,j}$ . These effects are characterized by the Doppler broadening full-width half-maximum (FWHM),  $\Delta\nu_D$  ( $\text{cm}^{-1}$ ), and the collisional broadening FWHM,  $\Delta\nu_C$  ( $\text{cm}^{-1}$ ), given by

$$\Delta\nu_D = 7.162 \times 10^{-7} \nu_0 \sqrt{\frac{T}{\hat{M}}} \quad (2a)$$

$$\Delta\nu_C = 2P \sum_i \chi_i \gamma_{i,0} \left(\frac{T_0}{T}\right)^{n_i} \quad (2b)$$

where  $\nu_0$  ( $\text{cm}^{-1}$ ) is the transition linecenter,  $\hat{M}$  (g/mol) is the molecular mass,  $\gamma_{i,0}$  ( $\text{cm}^{-1}/\text{atm}$ ) is the collisional broadening coefficient of the  $i^{\text{th}}$  colliding species at reference temperature  $T_0$  (296 K throughout this work), and  $n_i$  is the temperature exponent of the broadening coefficients.

## 2.2. Scanned-WMS-2f/1f

Extensive information describing scanned-WMS can be found in [10,11], therefore only a brief overview is provided here. WMS involves modulating the laser injection current with a sinusoidal waveform of frequency  $f_m$  to tune the laser wavelength around the linecenter of an absorption feature. The interaction between the laser wavelength modulation and the absorption lineshape introduces frequency content appearing at harmonics of  $f_m$ . Since the Fourier coefficients at the harmonics are related to the absorption spectrum of the probed gas, they can be used to recover absorption information and, by extension, thermodynamic properties of the gas. In WMS-2f/1f, the second harmonic is used to detect the absorption transition while the first harmonic is used to normalize the signal to neutralize non-absorbing interference sources (e.g., due to beam steering). In peak-picking scanned-WMS, a separate low-amplitude sinusoidal scan with frequency  $f_s$ , typically much lower than  $f_m$ , is superposed onto the modulation waveform.

## 2.3. Determination of temperature and mole fraction

The calibration-free WMS model given by Sun et al. and Goldenstein et al. [10,12] was used to generate lookup tables of peak WMS-2f/1f signals of the target  $\text{H}_2\text{O}$  absorption transitions as a function of gas properties and known laser tuning parameters. Experimentally derived spectroscopic parameters for the targeted  $\text{H}_2\text{O}$  absorption transitions were used to simulate the absorption spectra needed to generate the lookup tables. With pressure known from simultaneous measurements using co-located pressure transducers, the measured WMS-2f/1f peaks were compared against simulations to

infer temperature and mole fraction using the following algorithm, variants of which are widely used throughout the literature (see [4] for example):

1. For the known  $P$  and a guessed  $T$ , determine the value for  $\chi_{\text{H}_2\text{O}}$  where the simulated WMS-2f/1f peak equals the measured peak using Newton's method.
2. Iterate on  $T$  using Newton's method until  $\chi_{\text{H}_2\text{O}}$  for both absorption transitions match each other within some tolerance ( $10^{-6}$  was used). The converged  $T$  and  $\chi_{\text{H}_2\text{O}}$  are stored as the measurement.

## 3. Sensor design

### 3.1. Wavelength selection

Selecting absorption transitions suitable for the RDE environment is crucial to the performance of the sensor. Selection criteria include strong absorbance, isolation from interfering transitions, and adequate sensitivity to changes in temperature across the operating envelope of the RDE. Simulations and prior experiments within the RDE used in [6,13] suggest a pressure range from 1 to 4 atm, temperature range from 700 to 1600 K, and  $\text{H}_2\text{O}$  mole fraction ranges between 5 and 20% at the sensor plane during each firing.

A key difficulty in the selection process is the short optical path lengths accessible to the single-ended sensor within the RDE combustion annulus, where the round-trip path is only 1.52 cm. Obtaining high measurement SNR within these short paths motivates the use of MIR absorption transitions that probe the strong fundamental vibrational bands of  $\text{H}_2\text{O}$ . Several researchers previously developed robust MIR LAS sensors for  $\text{H}_2\text{O}$  and temperature sensing in harsh combustion environments [6,9,14] using transitions near  $3920.06 \text{ cm}^{-1}$  (2551 nm) and  $4029.59 \text{ cm}^{-1}$  (2482 nm). Spectral simulations of these transitions indicate adequate spectral absorbances throughout the operating envelope of the RDE, allowing for sensitive detection of the two transitions at the design conditions. In addition, the lower state energies of these transitions differ by  $1957 \text{ cm}^{-1}$ , which enables sensitive measurements of temperature. These absorption transitions were chosen for this work because of these favorable characteristics.

Spectroscopic parameters for these absorption transitions were compiled from the HITEMP 2010 database [15] and from experimental studies in [6,14]. These parameters are passed into the WMS model described in Section 2.3 to infer temperature and mole fraction from the collected photodetector signals.

### 3.2. WMS tuning parameters selection

To further improve measurement SNR, the peak-picking scanned-WMS technique described in Section 2.2 was used. The benefits of scanned-WMS versus typical direct-absorption LAS are well documented [12,16]; these primarily include: (1) enhanced  $1/f$ -noise rejection by shifting absorption information to higher frequencies, (2) ability to frequency multiplex multiple lasers onto the same detector, and (3) precise knowledge of the mean laser wavelength is not needed.

Selecting appropriate parameters for laser injection-current tuning is key to the performance of WMS-based sensors. The methods described in [12,14,17] were used to select appropriate WMS tuning parameters, accounting for (1) minimized crosstalk between the harmonics of the frequency-multiplexed lasers, (2) modulation depths that maximize SNR at the average expected thermodynamic conditions, and (3) sufficiently large scan widths to account for pressure-induced linecenter shifts throughout the RDE thermodynamic envelope. The selection process at an average expected temperature and pressure of 1100 K and 2.2 atm yielded  $f_m$ 's of 100 and 122 kHz, modulation depths of 0.306 and 0.063  $\text{cm}^{-1}$ , and scan widths of 0.087 and 0.030  $\text{cm}^{-1}$  for the 2551 nm and 2482 nm lasers, respectively.  $f_s = 10$  kHz for both lasers to achieve a 20 kHz measurement rate, sufficient to resolve detonation cycle dynamics.

Simulations of the WMS signals within the RDE operating thermodynamic envelope indicate that the WMS- $2f$  signals are both maximized and weakly dependent on pressure and broadening coefficient near the mean expected pressure of 2.2 atm, demonstrating that the selection strategy yielded modulation depths that would lead to good SNR while being less sensitive to pressure and broadening coefficient uncertainties. Simulated crosstalk between the two lasers never exceeded 0.5% throughout the operating envelope, demonstrating that the selected scan widths are small enough to avoid introducing significant crosstalk yet large enough to account for pressure shift.

### 3.3. Experimental setup

#### 3.3.1. Rotating detonation engine

The NPS RDE is described in detail in [13]; only important details are presented here. The RDE is an annular combustor with inner and outer channel radii of 6.22 and 6.98 cm, respectively, yielding a round-trip optical path of 1.52 cm. During operation,  $\text{H}_2$  and air are fed into the RDE via orthogonal injectors evenly distributed throughout the circumference of the injector. For the results presented here, mass flow rates of air and  $\text{H}_2$  were varied from 0.29 to 0.33  $\text{kg}\cdot\text{s}^{-1}$  and 0.0028 to 0.0045  $\text{kg}\cdot\text{s}^{-1}$ , respectively, to reach global equivalence ratios ranging from 0.8 to 1.35. Detonation

was initiated via a  $\text{H}_2\text{-O}_2$  ignitor torch mounted adjacent to the RDE with separate ion gauges distributed axially along the RDE to independently verify the existence of a propagating detonation wave. The optical sensor was placed at an axial plane 7.6 cm downstream of the injectors, which is well beyond the extent of the detonation waves. High-speed (Kistler 603B1, 400 kHz) and fluidically-damped low-speed (Omega PX603-500G5V, 200 Hz) pressure transducers at the sensor plane were used to monitor pressure.

#### 3.3.2. Optical design and optimization

Figure 1 shows a schematic of the optical configuration used for the single-ended RDE diagnostic, split into two major sub-assemblies: the laser coupling and control assembly (left) and a cross-section view of the detection assembly (right). On the coupling and control assembly side, two distributed feedback diode lasers (Nanoplus GmbH) operating near 2551 and 2482 nm, each with approximately 10 mW of output intensity, provided single-mode light sources for  $\text{H}_2\text{O}$  and temperature measurements. ILX LDC-39427 laser controllers and National Instruments USB-6353 waveform generators were used to control and modulate the lasers. Beams from the two lasers were free-space coupled onto a 300  $\mu\text{m}$  diameter 2-to-1 multimode hollow-core silver-coated fiber bundle (Opto-Knowledge Systems, Inc.). The fiber bundle combines the beams onto closely packed, collinear lines-of-sight while isolating sensitive electronics from vibrations during RDE operation [18].

The output end of the fiber bundle was attached to a collimator within the detection assembly that included a lens (Thorlabs) used to shape the beams exiting the fiber bundle. A turning mirror directed the beams into the RDE combustion annulus, which interfaced with the detection assembly via a 2-degree wedged sapphire window mounted on an adaptor plug. Back-scattered radiation from the mirror-polished stainless steel RDE inner surface was transmitted back to the detection assembly to be focused onto the photodetector chip (Vigo Systems S.A.) via a  $f = 20$  mm lens (Thorlabs). Optical emission from the hot combustion gases was suppressed with a 2.2-2.6  $\mu\text{m}$  bandpass filter (Spectrogon) and spatial filters. A data acquisition system (Pico Technologies) recorded voltages from the photodetector and pressure transducers. During post-processing, pressure measurements were synchronized based on the peak of the locally weighted cross-correlation between the photodetector and pressure signals (optical emission and pressure are positively correlated). This compensates for lag due to the 79-degree azimuthal offset between the sensor and pressure transducers and creates a more faithful representation of the actual gas pressure probed by the sensor.

The single-ended strategy has several unique optical design challenges, summarized as follows: (1)

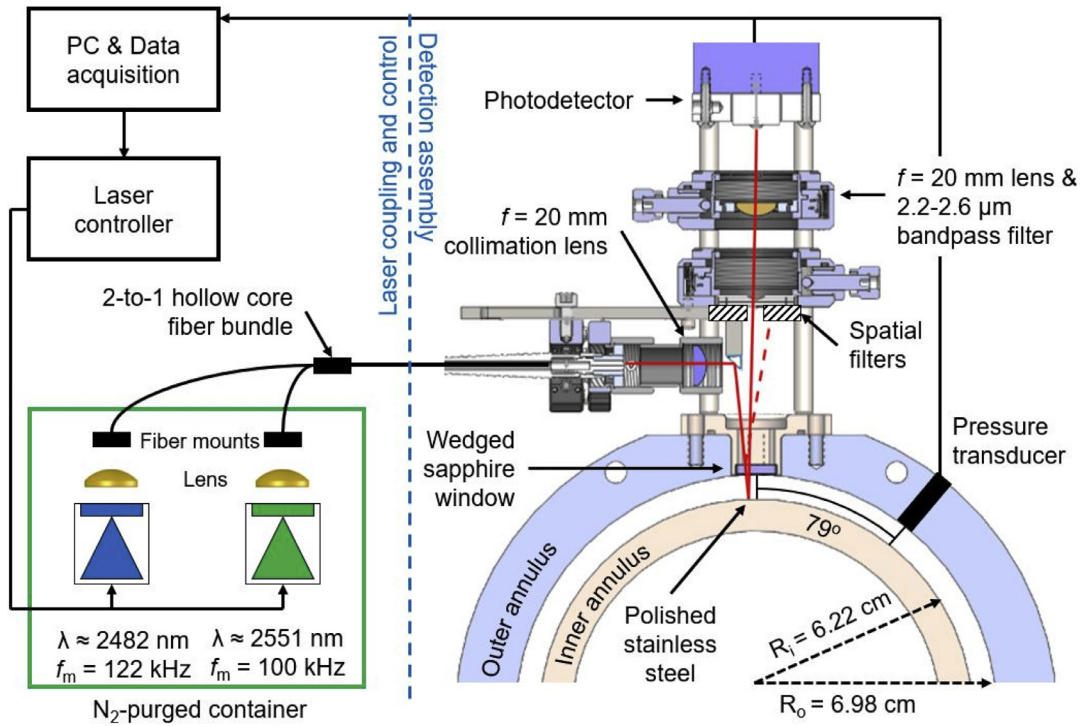


Fig. 1. Schematic of the numerically optimized single-ended optical setup with major elements labeled. Solid and dotted lines emanating from the fiber bundle represent the centerlines of the detection and unwanted window reflection, respectively.

The surfaces of the sapphire window reflect a component of the laser beams without ever interacting with the probed gas stream. If captured by the photodetector, these window reflections can introduce measurement errors. (2) The inner RDE surface may not be particularly efficient at reflecting laser light back into the detection assembly, especially when tarnished after multiple firings. Early sensing attempts by the authors yielded photodetector voltage traces that were overwhelmed by optical emission, rendering the measurements unusable. It is therefore crucial to design a detection configuration that both maximizes the laser-to-emission intensity ratio and remains tolerant to beam steering.

A ray-tracing numerical optimization algorithm was implemented to address the preceding challenges. The algorithm takes the positions of the optical elements within the detection assembly (e.g., distance between the collimation lens and the fiber tip) and computes the evolution of the beam (including position and  $1/e^2$  Gaussian beam diameter) using matrix optics [19]. Initial complex beam parameters at the fiber tip were experimentally characterized with a knife-edge. A separate loop evaluated the ray-tracing results for all possible permutations of the optical configuration and selected the arrangement that minimized the sum of the beam diameters at the spatial filter plane and at the

photodetector chip while rejecting cases that had physically blocked beams or detected unwanted reflection from the sapphire window. The beam diameter at the spatial filter plane was included in the optimization objective to minimize the solid angle of optical emission.

The solid and dotted curves emanating from the fiber bundle in Fig. 1 represent the centerlines of the detection beam and the unwanted window reflection, respectively, for the optimal optical configuration. Beam diameters at the spatial filter plane and the photodetector were on average  $8.73 \times 10^{-1}$  and  $6.3 \times 10^{-2}$  mm, respectively. Because the beam diameters at the photodetector are significantly smaller than the chip size of 0.2 cm, the sensor is desensitized to beam steering effects. With the optimal configuration implemented on the actual sensor hardware, the photodetector collected approximately twice as much laser intensity from each laser as an optical configuration optimized via trial-and-error. Similarly, the spatial filters rejected 82% of the optical emission emanating from a laboratory propane torch flame without loss in laser intensity. Together, optimization and spatial filtering improved the laser intensity-to-emission ratio by a factor of eleven as compared to previous configurations optimized via trial-and-error. Assuming beam steering and optical emission are broadband

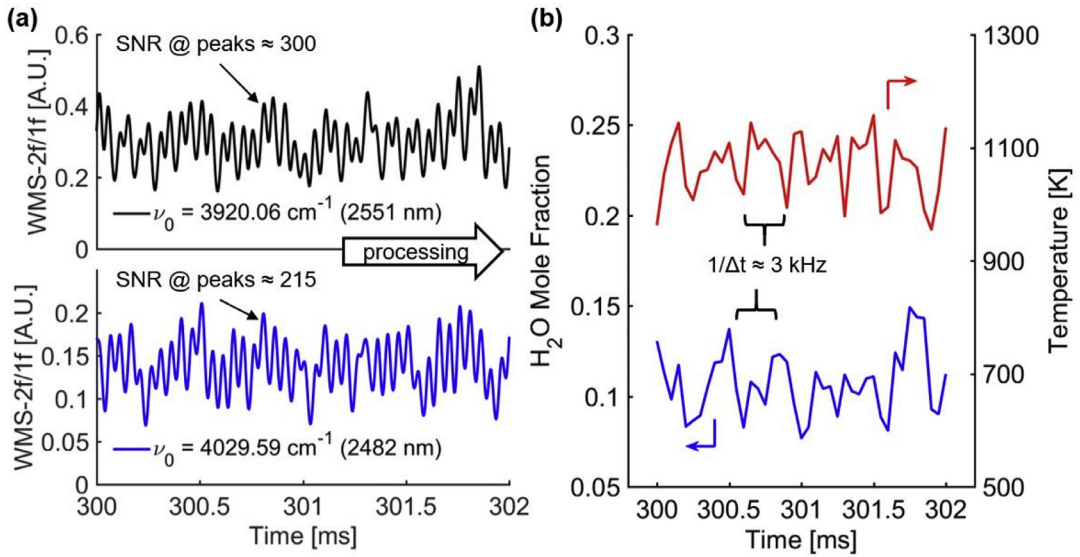


Fig. 2. (a) WMS-2f/1f signals for the probed absorption transitions and (b) post-processed temperature and H<sub>2</sub>O mole fraction for a period of 2 ms during quasi-steady-state RDE operation at  $\Phi_{\text{global}} = 1.26$ .

features in the frequency domain (this is true for the impulse-like shock structures that form downstream of the detonation wave within the RDE), this improvement theoretically corresponds to an eleven-fold increase in measurement SNR.

## 4. Results

### 4.1. Time-resolved dynamics

Figure 2 presents time-resolved results from a single RDE firing at  $\Phi_{\text{global}} = 1.26$ . Figure 2a shows the measured WMS-2f/1f signals as a function of time over a period of 2 ms after the RDE has reached quasi-steady-state. Each peak within the WMS-2f/1f signals represents a single measurement. An effective measurement rate of 20 kHz was achieved as the laser scans across the absorption transition twice per period of the 10 kHz scan. Figure 2b shows the post-processed temperature and H<sub>2</sub>O mole fraction measurements for the same 2 ms period, with clear oscillations of both mole fraction and temperature at  $\sim 3 \text{ kHz}$  corresponding to the detonation cycle frequency. Measurement noise was conservatively estimated using the frequency-domain noise reconstruction strategy utilized in [9], resulting in SNRs of approximately 300 and 215 for the  $3920.06 \text{ cm}^{-1}$  (2551 nm) and  $4029.59 \text{ cm}^{-1}$  (2482 nm) transitions, respectively, during this 2 ms period. Assuming a SNR of 10 is required to make meaningful measurements and that SNR scales linearly with mole fraction in the optically-thin environments here, the detection

limit of this sensor is approximately 0.5% H<sub>2</sub>O by mole.

Meaningful insights into the dynamics within the combustor can be visualized by taking short-time Fourier transforms (STFT) of the temperature and mole fraction time-histories. Figure 3 shows the H<sub>2</sub>O mole fraction (top row) and temperature (3rd row) STFTs for three RDE firings at  $\Phi_{\text{global}} = 0.87$  (left column), 1.09 (center column), and 1.35 (right column). The tone-mapping indicates the squared-magnitudes of the Fourier coefficients, with brighter tones representing stronger harmonics. These STFTs were generated using moving 50-ms Gaussian windows, which optimizes the tradeoff between time and frequency resolution. The second and fourth rows of Fig. 3 show the STFT (logarithmic-scale) at  $t = 500 \text{ ms}$  after ignition to emphasize the relative magnitudes of the harmonic components after the combustor has reached quasi-steady-state. Several trends can be extracted from Fig. 3:

1. The primary detonation mode can be seen near 3 kHz for  $\Phi_{\text{global}} = 1.09$  and 1.35. For  $\Phi_{\text{global}} = 0.87$ , the primary detonation mode shifts from a 3 kHz mode to a 3.25 kHz mode near 350 and 700 ms after ignition but quickly reverts to the 3 kHz mode within a few tens of milliseconds. These mode transitions demonstrate the possibility of multi-modal RDE combustion dynamics, contrasting with the typical view that RDEs operate with constantly-propagating quasi-steady detonation waves.

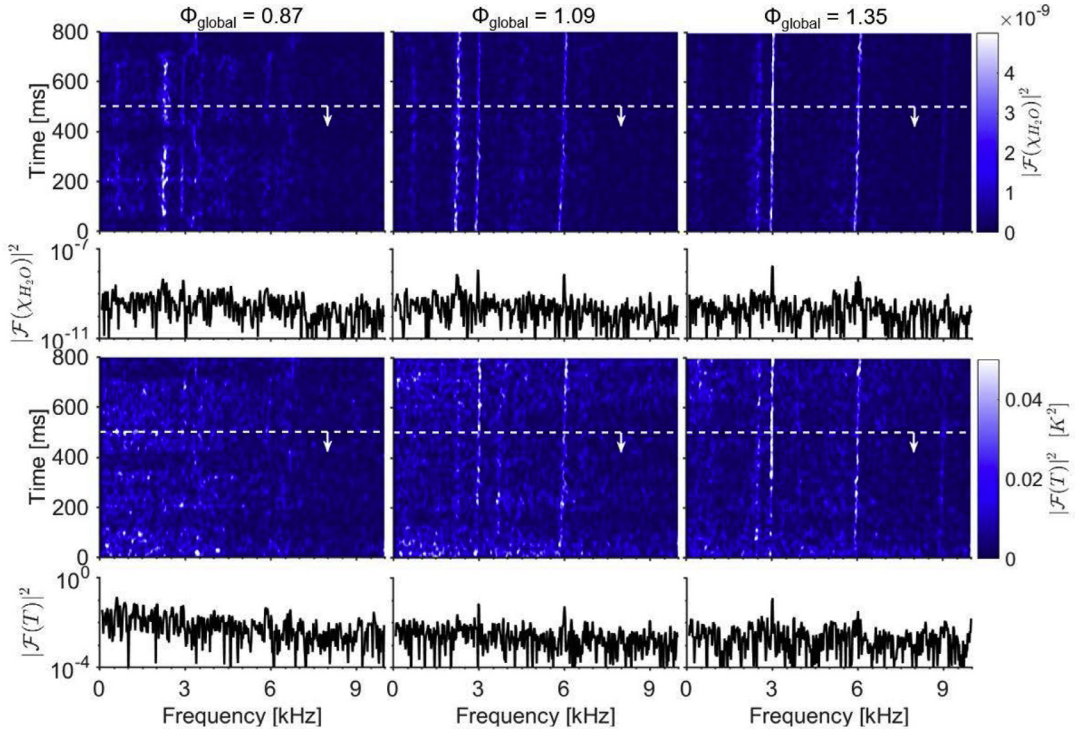


Fig. 3. Short-time Fourier transform (STFT) coefficients of the  $\text{H}_2\text{O}$  mole fraction (top row) and temperature (3rd row) time-histories for three RDE firings at  $\Phi_{\text{global}} = 0.87$  (left column), 1.09 (center column), and 1.35 (right column). Fourier transform slices 500 ms after ignition are shown below each STFT.

- At lower  $\Phi_{\text{global}}$ , the primary detonation mode near 3 kHz competes against the natural RDE acoustic mode near 2.3 kHz, which is especially apparent at  $\Phi_{\text{global}} = 1.09$ . As  $\Phi_{\text{global}}$  increases, the detonation mode overtakes and eventually dominates the acoustic mode.
- The primary harmonic near 3 kHz increases in frequency at an average rate of 129 Hz/s for all RDE firings, equal to 54 m/s<sup>2</sup> using the mean annular circumference. This is consistent with gradual heating of the combustor walls, leading to higher detonation velocities due to reduced heat transfer.

#### 4.2. Time-averaged metrics

Tests were conducted with multiple  $\text{H}_2/\text{air}$  mixture ratios to investigate the effects of equivalence ratio on temperature and composition. Figure 4a shows time-averaged temperatures and  $\text{H}_2\text{O}$  mole fractions for the seven measured RDE firings. Vertical bars representing  $\pm 1\sigma$  of the measurements over the quasi-steady test time of 0.8 s were overlaid on each measurement. Both mean temperature and  $\text{H}_2\text{O}$  mole fraction were weak functions of equivalence ratio, with temperatures falling within an 80 K range and mole fractions within a 2%

range. Temperature standard deviations were consistent with measurements by Rein et al. at a similar plane along an RDE with nearly identical dimensions [8].

Figure 4b shows the time-averaged combustion progress at the measurement plane, defined as the measured  $\text{H}_2\text{O}$  mole fraction over the local thermodynamic equilibrium  $\text{H}_2\text{O}$  mole fraction expected for each  $\Phi_{\text{global}}$ , and detonation wave velocity ( $v_{\text{wave}}$ ) normalized by the Chapman-Jouguet ( $v_{\text{CJ}}$ ) detonation velocity.  $v_{\text{wave}}$  was calculated using the detonation cycle frequency multiplied by the average circumference of the annulus while  $v_{\text{CJ}}$  was calculated using the enthalpy of reaction weighted by the combustion progress assuming no heat transfer. Combustion progress on the order of 35% is seen for all equivalence ratios except for the lean firings ( $\Phi_{\text{global}} = 0.8$  and 0.87), while  $v_{\text{wave}}$  is on average 83% of  $v_{\text{CJ}}$  with the discrepancy attributable to heat transfer losses.

The low combustion progress and weak temperature and mole fraction dependence on  $\Phi_{\text{global}}$  suggest mixing-limited combustion near the injection plane. Because the  $\text{H}_2$  and air are injected orthogonally into the combustor, it is likely that  $\text{H}_2$  and air remain stratified with only a relatively thin layer of well-mixed charge sustaining the detonation wave, leaving unburnt  $\text{H}_2/\text{air}$  pockets free to travel along



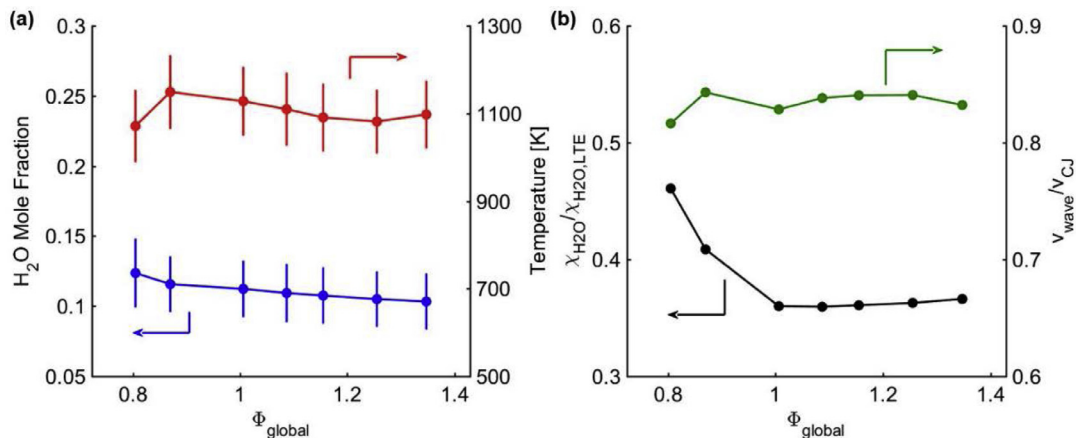


Fig. 4. Time-averaged (a)  $\text{H}_2\text{O}$  mole fraction and temperature and (b) combustion progress and detonation wave velocity normalized by the Chapman-Jouguet velocity as functions of global equivalence ratio. Vertical bars represent  $\pm 1\sigma$  measurement fluctuations over the quasi-steady-state test time of 0.8 s.

the combustor. For the lean  $\Phi_{\text{global}}$  firings (0.8 and 0.87), approximately the same amount of  $\text{H}_2$  and air are mixed and detonated as compared to the rich  $\Phi_{\text{global}}$  conditions, but because less  $\text{H}_2$  is injected for the lean firings, the combustion progress for these cases is higher. Note that combustion progress is a localized measurement upstream of the combustor exit and does not reflect overall RDE combustion efficiency. Additionally, the sensor was developed and tested on an early RDE configuration while a next generation RDE was being developed. In the future, the sensor will be deployed on the new RDE where enhanced injectors are expected to promote mixing and improve combustion progress at a comparable axial location.

### 4.3. Uncertainty analysis

Several sources contribute to the uncertainty of the measured temperatures and mole fractions: (1) Uncertainty in the spectroscopic parameters used to simulate the WMS-2f/1f peak lookup tables, (2) uncertainty in the pressure measurements, (3) unknown amounts of  $\text{H}_2$ ,  $\text{O}_2$ , and trace species in the gas stream leading to uncertain broadening coefficients, and (4) line-of-sight nonuniformities leading to uncertain path-averaged results. These contributions to the measurement uncertainty were estimated via the uncertainty propagation formula  $\sigma_a = \sqrt{\sum_p \sigma_p^2 \left(\frac{\partial a}{\partial p}\right)^2}$ , where  $a$  is either mole fraction or temperature,  $p$  are the sources of uncertainty, and  $\sigma$  represents uncertainty. The partial derivatives were numerically estimated by perturbing the WMS-2f/1f lookup tables with respect to each uncertain parameter.

Spectroscopic uncertainties are tabulated in [6,20] while pressure uncertainty is taken from

the manufacturers' quoted measurement uncertainties for the two separate transducers. The technique used in [6] was used to estimate uncertainty due to unknown bath gas composition, where the WMS lookup-table was recalculated for varying amounts of  $\text{H}_2$ ,  $\text{O}_2$  and assuming  $\gamma_{\text{H}_2} \approx 0.95\gamma_{\text{N}_2}$  and  $\gamma_{\text{O}_2} \approx 0.65\gamma_{\text{N}_2}$ . To account for line-of-sight non-uniformities, pressure and mole fraction are assumed to be uniformly distributed (a reasonable assumption for the small annular gap) and temperature conservatively took a parabolic distribution with wall temperatures equal to 600 K and mean temperature equal to the sensor-measured mean temperature. The WMS lookup-table was recalculated using this approximate temperature distribution to determine a conservative estimate of uncertainty due to non-uniformities.

At the mean thermodynamic condition of 1100 K, 2.2 atm, and 12%  $\text{H}_2\text{O}$  by mole, spectroscopic parameters contributed 4.8% and 3.3% uncertainty to measured  $\chi_{\text{H}_2\text{O}}$  and  $T$ , respectively, while pressure contributed 0.6% and 0.06%, bath gas composition contributed 1.7% and 0.2%, and LOS nonuniformity contributed 5.2% and 4.1%. These sources combined for an overall uncertainty of 7.3% and 5.3% for  $\chi_{\text{H}_2\text{O}}$  and  $T$ , respectively.

## 5. Conclusions

A novel single-ended LAS sensor was used to measure  $\text{H}_2\text{O}$  mole fractions and temperature within a  $\text{H}_2$ /air-fed RDE at 20 kHz. The design used strong MIR transitions near  $2.5 \mu\text{m}$  and scanned-WMS-2f/1f to enable high-SNR measurements with detection limits of 0.5%  $\text{H}_2\text{O}$  by mole despite the short optical path of 1.52 cm. Ray-tracing optimization was used to overcome

unique design challenges associated with the single-ended detection strategy. Results in an operating RDE identified competing detonation and acoustic modes and detonation velocities that increase with time. Time-averaged metrics indicate low combustion progress and mole fractions and temperatures that were weak functions of  $\Phi_{\text{global}}$ , consistent with mixing-limited combustion near the injector plane.

This work represents the first use of a single-ended MIR sensor in a harsh engine environment and demonstrates the utility of this diagnostic not just for RDE design, but also in a variety of other applications where installing direct optical paths is not practical. Key requirements for applying this approach to other devices include the following: (1) selecting appropriate laser absorption transitions for the target application, (2) identifying suitable surfaces within the device for back-reflection (e.g., surfaces with adequate specular reflectivity and are geometrically oriented to reflect laser beams into the photodetection assembly), (3) ray-tracing the optical system to maximize laser intensity-to-emission ratio, and (4) using interference-tolerant spectroscopic techniques such as WMS to overcome systems with poor optical throughput (e.g., due to poor or tarnished back-scattering surfaces).

## Acknowledgments

Sponsors: Office of Naval Research (Grant No. N00014-15-P-1121) and Innovative Scientific Solutions Incorporated (ISSI). W.Y. Peng and S.J. Cassady were supported by the National Defense Science and Engineering Graduate (NDSEG) Fellowship, 32 CFR 168a awarded by DoD, Air Force Office of Scientific Research and Army Research Office. The authors would like to thank J. Hoke of ISSI for monitoring the contract and D. Dausen of NPS for hosting the measurement campaign and operating the RDE.

## References

- [1] F.K. Lu, E.M. Braun, *J. Propuls. Power* 30 (5) (2014) 1125–1142.
- [2] F.A. Bykovskii, S.A. Zhdan, E.F. Vedernikov, *J. Propuls. Power* 22 (6) (2006) 1204–1216.
- [3] C.S. Goldenstein, R.M. Spearrin, J.B. Jeffries, R.K. Hanson, *Prog. Energy Combust. Sci* 60 (2016) 132–176.
- [4] C.S. Goldenstein, R.M. Spearrin, J.B. Jeffries, R.K. Hanson, *Proc. Combust. Inst.* 35 (3) (2014) 3739–3747.
- [5] I.A. Schultz, C.S. Goldenstein, J.B. Jeffries, R.K. Hanson, R.D. Rockwell, C.P. Goyne, *J. Propuls. Power* 30 (3) (2014) 550–557.
- [6] C.S. Goldenstein, C.A. Almodóvar, J.B. Jeffries, R.K. Hanson, C.M. Brophy, *Meas. Sci. Technol* 25 (10) (2014) 1–11.
- [7] K.D. Rein, S. Roy, B.C. Sell, et al., *AIAA SciTech Forum* (2016).
- [8] K.D. Rein, S. Roy, J.L. Hoke, A.W. Caswell, F.R. Schauer, J.R. Gord, *AIAA SciTech Forum* (2017).
- [9] W.Y. Peng, C.S. Goldenstein, R.M. Spearrin, J.B. Jeffries, R.K. Hanson, *Appl. Opt.* 55 (33) (2016) 9347–9359.
- [10] C.S. Goldenstein, C.L. Strand, I.A. Schultz, K. Sun, J.B. Jeffries, R.K. Hanson, *Appl. Opt.* 53 (3) (2014) 356–367.
- [11] C.L. Strand, *Scanned Wavelength Modulation Absorption Spectroscopy with Application to Hypersonic Impulse Flow Facilities*, Ph.D Thesis, Stanford University, 2014.
- [12] K. Sun, X. Chao, R. Sur, C.S. Goldenstein, J.B. Jeffries, R.K. Hanson, *Meas. Sci. Technol* 24 (12) (2013) 1–12.
- [13] D.F. Dausen, C.M. Brophy, R.G. Wright, J.D. Marder, Design of an optically-accessible rotating detonation engine, *48th AIAA/ASME/SAE/ASEE Joint Propulsion Conference and Exhibit*, 2012.
- [14] C.S. Goldenstein, R.M. Spearrin, J.B. Jeffries, R.K. Hanson, *Appl. Phys. B Lasers Opt* 116 (3) (2014) 705–716.
- [15] L.S. Rothman, I.E. Gordon, R.J. Barber, et al., *Spectrosc. Radiat. Transf* 111 (15) (2010) 2139–2150.
- [16] P. Kluczynski, O. Axner, *Appl. Opt.* 38 (27) (1999) 5803–5815.
- [17] G.B. Rieker, J.B. Jeffries, R.K. Hanson, *Appl. Opt.* 48 (29) (2009) 5546–5560.
- [18] R.M. Spearrin, C.S. Goldenstein, I.A. Schultz, J.B. Jeffries, R.K. Hanson, *Appl. Phys. B* 117 (2) (2014) 689–698.
- [19] E. Hecht, *Optics*, 4th ed., Pearson Education Ltd., Harlow, U.K., 2002.
- [20] C.S. Goldenstein, J.B. Jeffries, R.K. Hanson, *J. Quant. Spectrosc. Radiat. Transf.* 130 (2013) 100–111.